

Is there a dynamical tendency in H_0 with late time measurements?

Mauricio Lopez-Henandez^a Josue De-Santiago^{a,b}

^aDepartamento de Física, Centro de Investigación y de Estudios Avanzados del I.P.N. Apartado Postal 14-740, 07000, Ciudad de México, México

^bConsejo Nacional de Humanidades, Ciencias y Tecnologías, Av. Insurgentes Sur 1582, 03940, Ciudad de México, México

E-mail: mauricio.lopez@cinvestav.mx, Josue.desantiago@cinvestav.mx

Abstract. The discrepancy between the Hubble constant H_0 values derived from early-time and late-time measurements, reaching up to 4σ , represents the most serious challenge in modern cosmology and astrophysics. In this work, we investigate if a similar tension exists between only late time measurements at different redshifts. We use the latest public datasets including Cosmic Chronometers, Megamasers, SNe Ia and DESI-BAO, that span from redshift $z \sim 0$ up to $z \sim 2.3$. By dividing the data into redshift bins, we derive H_0 values from each bin separately. Our analysis reveals a phenomenological dynamic evolution in H_0 across different redshift ranges, with a significance from 1.5σ and 2.3σ , depending on the parameterization. Consistency of the model demands observational constancy of H_0 since it is an integration constant within the Friedmann-Lemaître-Robertson-Walker (FLRW) metric. Thus, these findings suggest that the observed Hubble tension might not only exist between early and late-time measurements but also among late-time data themselves, providing new insights into the nature of the Hubble tension.

Contents

1	Introduction	1
2	Cosmology	2
3	Data	4
4	Fitting	4
5	Results	6
5.1	Quadratic parameterization	8
5.2	Fourier parameterization	8
5.3	Unbinned results	10
6	Summary and conclusions	11

1 Introduction

Our current understanding of the Universe relies on the Λ CDM model which incorporates the cosmological constant Λ and a cold dark matter component. This model is the most accepted and successful in explaining most cosmological observations [1, 2]. One of the most important challenges within the astrophysics and cosmology community is the discrepancy of more than 4σ for the Hubble constant H_0 , between local measurements using the cosmic distance ladder and early-time measurements of the cosmic microwave background (CMB). The former based on direct observations of Supernovae Type Ia (SNe Ia) calibrated with Cepheids by the SH0ES team [3] and the latter obtained by the Planck satellite, which relies on the Λ CDM model [1]. This so called **Hubble tension** has led to an exhaustive search for potential explanations. A wide range of models have been used to address the H_0 tension, proposing either a dark energy (DE) component during the early evolution of the Universe [4–9], a DE component with a time-varying equation of state [10–12], extra interactions between the components of the Universe [13–16], or modified gravity [17–19]. For a more comprehensive study about the H_0 tension and alternative proposals, see the reviews [20–22].

In the Λ CDM model, H_0 is a constant by definition: it represents the Hubble parameter $H(z)$ at the present epoch $H_0 = H(z = 0)$. However, recent results have shown that H_0 depends on the redshift of the probes used to determine it. The first of these results, from six gravitationally lensed quasars with measured time delays by the H0LiCOW program, indicated that H_0 decreases with lens redshift [23], with no evidence suggesting that this trend is due to unaccounted systematics [24]. Subsequent studies have found a similar feature in different datasets [25–34], offering a new perspective on the Hubble tension due to an apparent redshift dependence of a quantity that should, tautologically, be a constant.

Recently, the Dark Energy Spectroscopic Instrument (DESI) collaboration published its cosmological constraints from the first year of observations of baryon acoustic oscillations (BAO). The results favor models with a DE component whose equation of state varies with time by more than 2.6σ [35], which challenges the paradigm of what we previously believed to be correct in the Λ CDM model. This dynamical DE could be responsible for a H_0 that depends on redshift.

Ref. [25] found that splitting cosmological data in different redshift bins up to $z = 0.7$ gives different estimates to H_0 which are in contradiction with a single constant H_0 at 2.1σ level. Leading to the conclusion that the Hubble tension is present even between late time measurements themselves when taken at different redshifts. Ref. [25] assumed a cosmological constant and used BAO-BOSS data [2]. The new DESI results lead us to question whether the new data together with a dynamical DE could solve this tension.

The paper is organized as follows. In section 2, we detail the implemented methodology, along with the theory behind the cosmological probes used in this paper. In section 3, we mention the data used. In section 4, we explain the criteria used to split the data into bins. In section 5, we present our results on constraining the value of H_0 in each of the bins. Finally, the summary and conclusions can be found in section 6.

2 Cosmology

In light of the new discoveries for the first cosmological results from DESI [35], in this work we use a flat Universe with a dynamical Dark Energy component, with a Chevallier-Polarski-Linder (CPL) equation of state given by $w(a) = w_0 + w_a(1 - a)$ [36, 37]. The Friedmann equation is given by the following parameterization

$$H(z) = H_0 [\Omega_m(1+z)^3 + (1 - \Omega_m)f(z)]^{1/2}, \quad (2.1)$$

where

$$f(z) = (1+z)^{3(1+w_0+w_a)} e^{-3w_a z/(1+z)}, \quad (2.2)$$

and with H_0 , Ω_m , w_0 , w_a the free parameters.

Following [25], we will split different cosmological data according to their redshift in order to estimate the Hubble constant using only data in certain redshift ranges. This method involves binning a modern dataset that includes the new DESI data, cosmic chronometers (CC), megamasers, and SNe Ia samples. The SNe Ia samples comprises the Pantheon+ compilation, and the new Union3 compilation and Dark Energy Survey (DES) Year 5 data release. With this new data we were able to expand the redshift range in the analysis to observe in more depth the evolution of H_0 with the redshift of the data.

Cosmic chronometers provide a direct estimate of the expansion rate of the Universe. This method takes advantage of the fact that the Hubble parameter, $H(z)$, can be directly expressed as a function of the time differential of the Universe, dt , over a given redshift interval, dz [38]

$$H(z) = -\frac{1}{1+z} \frac{dz}{dt}. \quad (2.3)$$

CCs evolve homogeneously as a function of cosmic time and on a timescale much longer than their age difference. Given $H(z)$, to obtain H_0 from eq. (2.1) it is necessary to determine Ω_m , w_0 , w_a from other observations.

The water megamasers found in the accretion disks of supermassive black holes in active galactic nuclei (AGN) act like a laser beam in the microwave band, providing a method to calculate extragalactic distances without relying on the cosmic distance ladder [39]. The disk model returns an estimation of the angular diameter distance \hat{D}_A to the galaxy and its recession velocity \hat{v}_i . The decomposition of this velocity between its peculiar and cosmological components $\hat{v}_i = v_{\text{pec},i} + cz_i$ is unknown for objects this close. Each \hat{D}_A is related to its

expected redshift z_i and the cosmological parameters by the equation

$$D_A(z) = \frac{c}{1+z} \int_0^z \frac{dz'}{H(z')}. \quad (2.4)$$

Following [40], we take peculiar velocities of the galaxies into account incorporating $\sigma_{\text{pec}} = 250 \text{ km s}^{-1}$ into the velocity uncertainties. The chi-squared used to constrain cosmological parameters is then given as

$$\chi^2 = \sum_{i=1}^N \left[\frac{(v_i - \hat{v}_i)^2}{\sigma_{v,i}^2 + \sigma_{\text{pec}}^2} + \frac{(D_A(v_i/c) - \hat{D}_i)^2}{\sigma_{D,i}^2} \right], \quad (2.5)$$

where the expected cosmological recession velocities are given by $v_i = cz_i$, N the number of data, $\sigma_{v,i}$ is the statistical uncertainty in the velocity measurement \hat{v}_i , and $\sigma_{D,i}$ is the standard deviation of the distance measurement \hat{D}_i . We take the expected velocities v_i for megamaser host galaxies as nuisance parameters.

The SNe Ia data gives the apparent magnitude m_b of each SNe, which can be compared with the predicted model given by

$$m_b = M + \mu(z) = M + 25 + 5 \log_{10} \left(\frac{D_L(z)}{\text{Mpc}} \right), \quad (2.6)$$

where M is the absolute magnitude for SNe Ia, and $D_L(z)$ is the luminosity distance, which in the case of SNe Ia can be written, according to [41], by

$$D_L(z) = (1 + z_{\text{hel}})(1 + z_{\text{cmb}})D_A(z_{\text{cmb}}), \quad (2.7)$$

z_{hel} is the heliocentric redshift of the SNe (or its host galaxy) and z_{cmb} is this redshift corrected for the peculiar motion of the solar system with respect to the CMB. Note that the parameters M and H_0 are degenerate when analyzing SNe alone. Therefore, SNe measurements are used to constrain other cosmological parameters, particularly the matter density Ω_m .

The BAO measurements provide distances relative to the sound horizon, r_d , as a function of redshift [2]. Along the line-of-sight direction, a measurement of the redshift interval, Δz , gives a means to measure the Hubble distance at redshift z ,

$$D_H(z) = \frac{c}{H(z)}. \quad (2.8)$$

Along the transverse direction, measuring the angle $\Delta\theta$ subtended by the BAO feature at z estimates the comoving angular diameter distance, $D_M(z)$

$$D_M(z) = (1+z)D_A(z), \quad (2.9)$$

These measurements can also be summarized by a single estimation representing the spherically averaged distance

$$D_V(z) = [zD_M^2(z)D_H(z)]^{1/3}, \quad (2.10)$$

BAO measurements constrain these distances all divided by the sound horizon r_d . Therefore, H_0 and r_d are degenerated with each other. The BAO measurements constraint the product $H_0 r_d$, and therefore are key in the treatment of Hubble tension. This constraint implies that a higher H_0 , as that obtained by SH0ES [3], requires a lower r_d , which is incompatible with the value inferred by the Planck Collaboration [1]. In this work we won't use the CMB prior on r_d as this will imply the use of data outside our redshift bins.

3 Data

To constrain H_0 , we use the following public data up to the redshift $z < 2.33$, including their systematic errors and covariance matrices. These data correspond to the latest public measurements of the observables from the previous section:

- I. Distances and recession velocities from 6 megamasers in the range $0.002 \leq z \leq 0.034$, from the Megamaser Cosmology Project [39, 40, 42].
- II. 32 cosmic chronometers data in the range $0.07 \leq z \leq 2$, from refs. [43–51]. We estimate the covariance matrix¹ between these data points following ref. [52].
- III. BAO measurements in galaxy, quasar and Lyman- α forest tracers from the Year 1 data release of DESI. These are measurements of the transverse comoving distance D_M and Hubble rate D_H , or their combination D_V , relative to the sound horizon r_d with the following effective redshifts $z_{\text{eff}} = 0.30, 0.51, 0.71, 0.93, 1.32, 1.49, 2.33$ [35].
- IV. For the supernovae type Ia measurements, we use any of the three latest compilations. 1,590 SNe Ia from the Pantheon+ compilation in the redshift range $0.01 \leq z \leq 2.26$ [53]. Recently published results from the Year 5 data release of the Dark Energy Survey (DES Y5) that include 1,635 new photometrically classified SNe Ia and 194 low-redshift SNe Ia (which are also in common with Pantheon+), spanning $0.025 \leq z \leq 1.3$ [54]. Finally, 22 binned data points from 2087 SNe Ia from the Union3 sample in the range $0.05 \leq z \leq 2.26$ [55], which has 1360 SNe in common with Pantheon+. We include both the statistical and systematic uncertainties in the three sets. We emphasize that these SNe Ia data are not independent of each other, and therefore, we cannot combine them. However, they differ in the way they analyze systematic errors and astrophysical parameters, making it interesting to compare the results of each of them.

Compared with the data used in ref. [25] which includes the BOSS BAO data [2] and the Pantheon sample [56], we have the BAO data from DESI Y1, the recent supernovae compilations Pantheon+, Union3 and DES Y5, as well as three extra measurements of CC.

Since the Pantheon+, DES and Union3 data cannot be combined, we present each of their results separately. The analyses always include the megamasers+CC+DESI data, which we will call “Base”, but differ in the SNe sample. We denote each case as Base+PantheonPlus, Base+Union3 and Base+DES.

4 Fitting

In this section, we describe how we fit the cosmological parameters using the data specified in the last section. Our objective is to see if the estimation of the Hubble constant H_0 is consistent when using data at different redshifts. We will split the total redshift range from our data in separate redshift bins with $z \in (z_{\text{min}}^i, z_{\text{max}}^i)$ and we use only data coming from that bin to estimate H_0 .

The redshift width of the bins varies between each other as we follow the strategy used in [25] requiring that the average redshift of each bin coincides between megamasers, SNe and

¹The detailed recipe on how to correctly estimate the covariance matrix for cosmic chronometers is given in <https://gitlab.com/mmoresco/CCcovariance>

Base+PantheonPlus			
Bin	Data	Range	\bar{z}
1	Megamasers, SNe	$0.01 < z \leq 0.069$	0.032
2	SNe, CC	$0.069 < z \leq 0.199$	0.15
3	SNe, CC, DESI-BGS	$0.199 < z \leq 0.425$	0.30
4	SNe, CC, DESI-LRG1 ($z = 0.51$)	$0.425 < z \leq 0.625$	0.51
5	SNe, CC, DESI-LRG2 ($z = 0.71$)	$0.625 < z \leq 0.7891$	0.71
6	SNe, CC, DESI-LRG3+ELG1	$0.7891 < z \leq 1.13$	0.93
7	SNe, CC, DESI-ELG2, DESI-QSO	$1.13 < z \leq 1.65$	1.38
8	SNe, CC, DESI-Lya	$1.65 < z \leq 2.3$	1.94
Base+Union3			
Bin	Data	Range	\bar{z}
1	Megamasers, SNe	$0 < z \leq 0.069$	0.05
2	SNe, CC	$0.069 < z \leq 0.19$	0.12
3	SNe, CC, DESI-BGS	$0.19 < z \leq 0.44$	0.30
4	SNe, CC, DESI-LRG1 ($z = 0.51$)	$0.44 < z \leq 0.649$	0.51
5	SNe, CC, DESI-LRG2 ($z = 0.71$)	$0.649 < z \leq 0.79$	0.71
6	SNe, CC, DESI-LRG3+ELG1	$0.79 < z \leq 1.23$	0.93
7	SNe, CC, DESI-ELG2, DESI-QSO	$1.23 < z \leq 1.7$	1.36
8	SNe, CC, DESI-Lya	$1.7 < z \leq 2.3$	2.26
Base+DES			
Bin	Data	Range	\bar{z}
1	Megamasers, SNe	$0 < z \leq 0.069$	0.041
2	SNe, CC	$0.069 < z \leq 0.19$	0.12
3	SNe, CC, DESI-BGS	$0.19 < z \leq 0.401$	0.30
4	SNe, CC, DESI-LRG1 ($z = 0.51$)	$0.401 < z \leq 0.63$	0.51
5	SNe, CC, DESI-LRG2 ($z = 0.71$)	$0.63 < z \leq 0.826$	0.71
6	SNe, CC, DESI-LRG3+ELG1	$0.826 < z \leq 1.13$	0.93

Table 1: Summary of the data, range in redshift and \bar{z} in each bin for each different data set.

BAO. We use the weighted average \bar{z} given by

$$\bar{z}_i = \frac{\sum_k^{N_i} z_k (\sigma_k)^{-2}}{\sum_k^{N_i} (\sigma_k)^{-2}}, \quad (4.1)$$

where N_i denotes the number of data used in the bin i and σ_k denotes the error in the observable at redshift z_k . For megamasers we use $\sigma_k^2 = \sigma_{v,k}^2 + \sigma_{\text{pec}}^2 + \sigma_{D,k}^2$. The bins constructed in each analysis are summarized in table 1.

Not all bins contain all the data. The megamasers appear only in the first redshift bin, while some bins lack DESI data. We only require that all bins contain either CCs or megamasers to break the degeneracies needed to obtain a value of H_0 . We emphasize that the condition (4.1) leads to different binnings and different \bar{z} 's depending on the SNe's used (PantheonPlus, Union3 and DES).

Data	$H_0 \left[\frac{\text{km}}{\text{s Mpc}} \right]$							
	Bin 1	Bin 2	Bin 3	Bin 4	Bin 5	Bin 6	Bin 7	Bin 8
Base+PantheonPlus	$73.32^{+3.34}_{-2.92}$	$67.84^{+5.37}_{-5.20}$	$66.08^{+5.26}_{-5.11}$	$56.24^{+6.91}_{-6.36}$	$67.19^{+8.92}_{-7.82}$	$78.86^{+10.30}_{-8.62}$	$64.32^{+10.24}_{-7.91}$	$64.16^{+15.82}_{-12.51}$
Base+Union3	$73.38^{+3.12}_{-2.82}$	$63.35^{+5.58}_{-5.03}$	$66.88^{+5.26}_{-5.17}$	$59.20^{+7.26}_{-6.53}$	$65.12^{+8.86}_{-7.63}$	$79.14^{+10.38}_{-9.13}$	$64.03^{+9.69}_{-8.14}$	$66.11^{+14.32}_{-11.77}$
Base+DES	73.43 ± 2.97	$65.67^{+5.97}_{-5.52}$	$63.04^{+5.41}_{-5.11}$	$61.78^{+6.45}_{-5.99}$	$66.36^{+8.37}_{-8.09}$	$77.04^{+9.79}_{-9.02}$	–	–

Table 2: Numerical values for the best-fit H_0 in each bin and for each data set. To see the redshift range of each of the bins refer to table 1. This data is plotted in fig. 1.

To fit the parameters, we used the Python module *emcee* [57]. We set flat priors for all the parameters, in particular for H_0 the prior is large enough that its fitting is mainly influenced by the measurements

$$H_0 \in (0, 150). \quad (4.2)$$

On the other hand, the data contained in a single bin lack the power to constrain the equation of state parameters w_0 and w_a . Therefore the posteriors of these parameters are mainly influenced by their priors. We considered large prior ranges

$$w_a \in (-2.5, 2.5), \quad w_0 \in (-1.5, -1/3), \quad (4.3)$$

to allow for enough freedom in the DE dynamics. These ranges contain both the DESI estimation² and the cosmological constant $w_0 = -1$, $w_a = 0$. After we fit the parameters, w_0 and w_a take values in their entire allowed region without preference for a particular value. This comes from the narrow ranges in z for each bin which limit the evolution of $f(z)$ in equation (2.2) and therefore the possible observable effects from a dynamical Dark Energy. In subsection 5.3 we do find limits for w_0 and w_a using the full redshift range of the data.

Not all bins fit all parameters due to the fact that each bin may or may not contain a certain type of data. The only parameters fitted in all bins are Ω_m , H_0 , w_0 , w_a , and the absolute magnitude of SNe Ia M .

5 Results

We show the fitted values of H_0 for each bin in Table 2 and illustrate them in figure 1. In all three analyses, H_0 decreases as function of redshift for $z < 0.6$, which agrees with [25]. In the next two bins, the value of H_0 increases to a maximum of $\sim 78 \text{ km s}^{-1} \text{ Mpc}^{-1}$ and then decreases again. Note that the scarcity and low quality of data inflate the errors at high redshifts.

In figure 1 we see that the estimations in H_0 seem to depend on the redshift. In order to quantify how much this measurements deviate from a constant, we introduce different parameterizations

$$\tilde{H}_0(\bar{z}, \theta_k), \quad (5.1)$$

that are functions of the redshift of the measurements \bar{z} and some parameters θ_k for $k = 1, 2, \dots$ which allow \tilde{H}_0 to deviate from a constant. Assuming statistical independence we

²We recall that $w_0 = -0.64 \pm 0.11$, and $w_a = -1.27^{+0.40}_{-0.34}$ for DESI+CMB+Union3 [35].

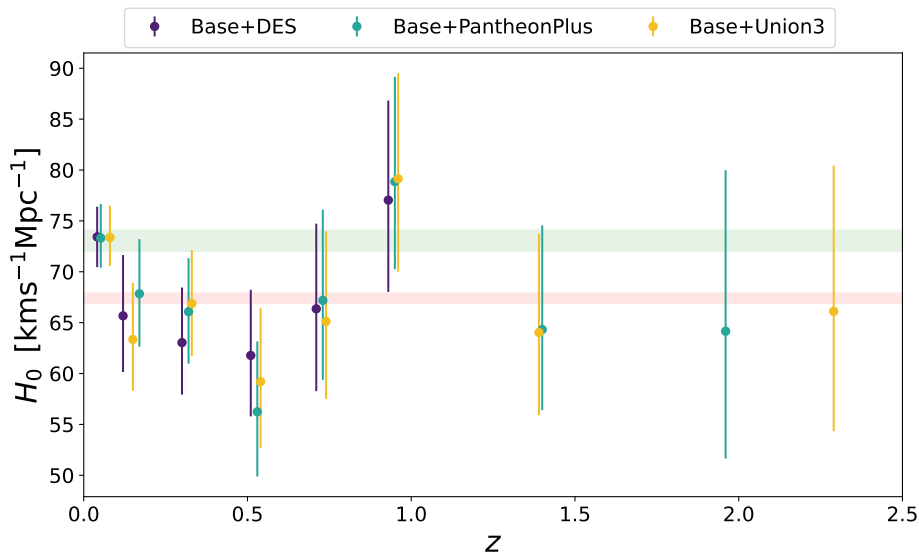


Figure 1: Best-fit values for the Hubble constant in each bin and for each different data set. The Base+DES data cover the range $z \leq 1.3$, so it includes only 6 redshift bins, compared to Base+PantheonPlus and Base+Union3, which cover a wider range. For a better visibility, we shifted the redshift centers $\bar{z}_i + 0.02$ for Base+PantheonPlus and $\bar{z}_i + 0.03$ for Base+Union3. The centers of the bins \bar{z}_i differ for each data set due to eq. (4.1). The green horizontal band corresponds to the value from SH0ES [3] ($H_0 = 73.04 \pm 1.04 \text{ km s}^{-1} \text{Mpc}^{-1}$) and the light red horizontal band corresponds to the value from Planck 2018 [1] within a Λ CDM scenario ($H_0 = 67.4 \pm 0.5 \text{ km s}^{-1} \text{Mpc}^{-1}$).

compute the total posterior as

$$P_{\text{tot}}(\theta_k) = \prod_{i=1}^{i_{\text{max}}} P_i(\tilde{H}_0(\bar{z}_i, \theta_k)), \quad (5.2)$$

where the posteriors P_i result from the fits of each of the bins. With this, we fit the parameters θ_k and estimate how much \tilde{H}_0 deviates from a constant.

We evaluate how statistically significant is the deviation from a constant H_0 by using three different methods. First, we use the Bayesian evidence given by [58]

$$E = \int \Pi(\theta_k) \mathcal{L}(\theta_k) d\theta_k, \quad (5.3)$$

where Π is the prior and \mathcal{L} the Likelihood of the parameters θ_k . We compute the integral using the nested integration algorithm Polychord [59, 60]. Here a larger value means a model with more probability. We report the Bayes factor given by

$$B = \frac{E_{\text{var}}}{E_{\text{cons}}} \quad (5.4)$$

and use it to determine if either the variable model or the constant is favored by the data.

Secondly, the Akaike Information Criterion (AIC) defined as [61, 62]

$$\text{AIC} = -2 \log \mathcal{L}_{\text{max}} + 2k, \quad (5.5)$$

where \mathcal{L}_{max} is the maximum likelihood that can be obtained within the model and k the number of free parameters. Between the two models, the variable and the constant, the

one with the smaller AIC value is preferred by the data. This criterion favors the larger \mathcal{L}_{\max} but penalizes too many extra parameters. In the next subsections we report $\Delta\text{AIC} = \text{AIC}_{\text{var}} - \text{AIC}_{\text{cons}}$.

Thirdly, we determine the number of standard deviations (σ) away from a constant. For parameterizations with a single extra parameter we only divide the distance to a constant by the standard deviation of the parameter. For models with more parameters, we compute the p -value of the variable model and, assuming a Gaussian distribution, we determine the number of standard deviations associated with that p -value. This is the least rigorous of our tests, but serves to communicate the relevance of our results as the cosmological community is familiar with the concept that a few σ 's can be the result of statistical fluctuations and not a physical effect.

5.1 Quadratic parameterization

The first 6 bins in figure 1 seem to indicate a quadratic behaviour, therefore we propose a quadratic parameterization of the form

$$\tilde{H}_0(z) = \hat{H}_0 + mz + bz^2, \quad (5.6)$$

with parameters \hat{H}_0 , m and b . For the fit, we exclude the results for bins 7 and 8 in order to avoid biases caused by the abrupt drop in the value of H_0 in bin 7, and the large error bars in bin 8.

The results are shown in table 3 and in figure ??, which displays the best fit to this quadratic function. We also drew the 2.3, 16, 84 and 97.7 percentiles of the fitted samples as a function of redshift to represent the 1σ and 2σ errors.

From the table 3 we can see that the parameters m and b deviate from zero, favouring a non constant H_0 model. The values of the Bayes factor and the ΔAIC however, show that this parametrization improves very modestly the fit to the data given by the constant H_0 . Only accounting for a barely worth mentioning result according to the Jeffreys' scale [63] of the Bayes factor. And according to the ΔAIC scale in [62] corresponding to no preference between the models.

It is evident that the low values of H_0 in the last two bins can lead to a fitting which is compatible with a constant H_0 ($m = 0$ and $b = 0$). This can be considered a limitation of the quadratic parameterization, which asks for H_0 to grow up to infinity at large redshifts. As this parameterization is purely phenomenological, we change it for one that won't present this behaviour in the next subsection.

5.2 Fourier parameterization

If we consider all the bins in figure 1, we see a possible oscillatory behavior. Therefore, we follow ref. [64] by proposing a parameterization in terms of the Fourier series

$$\tilde{H}_0(z, b_k, c_k) = \hat{H}_0 + \sum_k [b_k \sin(2k\pi a) + c_k \cos(2k\pi a)], \quad (5.7)$$

where $a = 1/(1+z)$ is the scale factor. After fitting different cuts of the series, we have obtained that the second term in the cosine series c_2 follows the oscillatory trend particularly well. In order to simplify the parameterization we stay with

$$\tilde{H}_0(z) = \hat{H}_0 + A \cos(4\pi a). \quad (5.8)$$

Data	$\hat{H}_0 \left[\frac{\text{km}}{\text{s Mpc}} \right]$	$m \left[\frac{\text{km}}{\text{s Mpc}} \right]$	$b \left[\frac{\text{km}}{\text{s Mpc}} \right]$	σ	ΔAIC	B
Base+PantheonPlus	$75.18^{+3.76}_{-3.42}$	$-65.96^{+26.31}_{-26.69}$	$72.27^{+31.63}_{-30.81}$	1.5	-1.67	1.59
Base+Union3	$75.06^{+3.79}_{-3.47}$	$-63.98^{+29.04}_{-28.90}$	$70.32^{+34.48}_{-33.89}$	1.3	-0.70	1.30
Base+DES	$74.64^{+3.62}_{-3.36}$	$-64.89^{+26.68}_{-26.49}$	$71.83^{+32.00}_{-32.08}$	1.5	-1.52	1.72

Table 3: Constraints on the parameters \hat{H}_0 , m and b in the quadratic parameterization (5.6) for the first 6 bins. We compared the model to a constant H_0 and determine the Bayes factor B , ΔAIC and σ deviation. While the σ values favors a dynamic H_0 , the Bayes factor indicates only a barely worth mentioning preference for the quadratic model, and the ΔAIC shows no preference between them, as determined using the scale provided by [62].

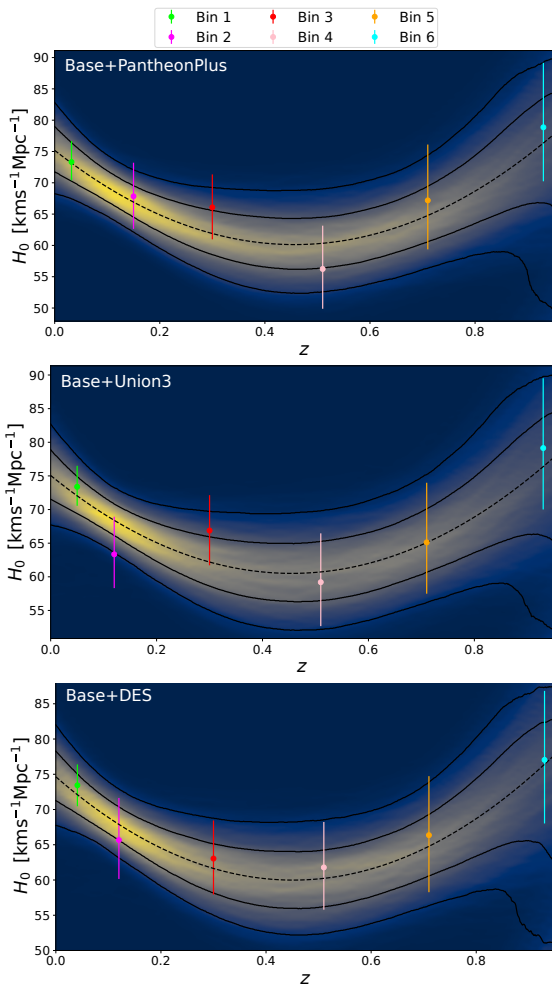


Figure 2: The fit of the quadratic function (5.6) against the binned results for H_0 in the Base+PantheonPlus sample, Base+Union3 sample and Base+DES sample. The dashed line represents the best fit, while the external solid lines represent the 1σ and 2σ errors. For this parametrization we only use the first 6 bins of each data set.

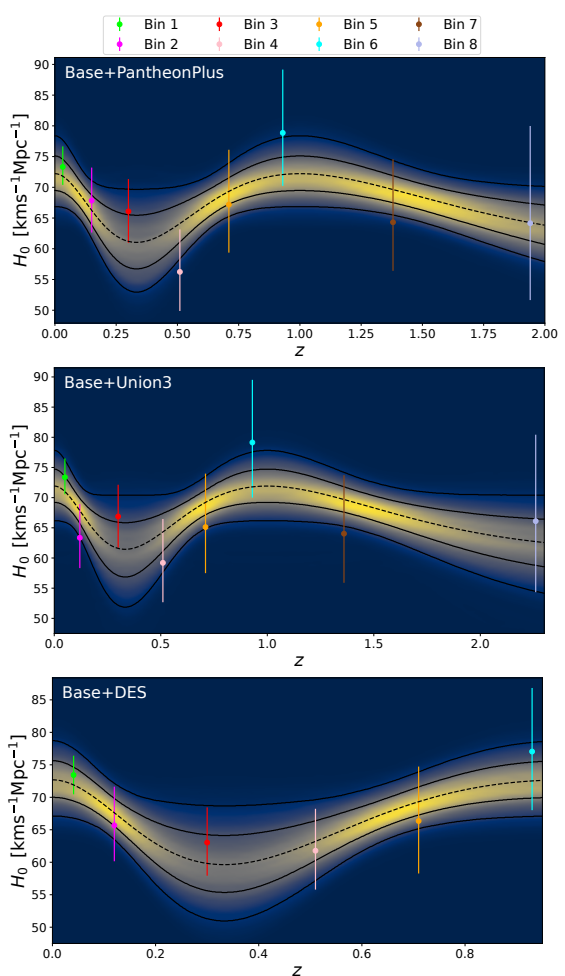


Figure 3: The fit to the Fourier parameterization (5.8) against the binned results for H_0 in the Base+PantheonPlus sample, Base+Union3 sample and Base+DES sample. Recall that Base+DES only has 6 bins. The dashed line represents the best fit, while the external solid lines represent the 1σ and 2σ errors.

Data	$\hat{H}_0 \left[\frac{\text{km}}{\text{s Mpc}} \right]$	$A \left[\frac{\text{km}}{\text{s Mpc}} \right]$	σ	ΔAIC	B
6 bins					
Base+PantheonPlus	$67.15^{+2.40}_{-2.35}$	$5.70^{+2.82}_{-2.88}$	2	-1.90	2.11
Base+Union3	$67.10^{+2.34}_{-2.47}$	$5.35^{+3.08}_{-2.94}$	1.8	-1.22	1.90
Base+DES	$66.15^{+2.39}_{-2.19}$	$6.53^{+2.88}_{-2.85}$	2.3	-2.90	3.87
8 bins					
Base+PantheonPlus	$66.63^{+2.39}_{-2.27}$	$5.59^{+2.76}_{-2.78}$	2	-2.03	2.21
Base+Union3	$66.68^{+2.25}_{-2.34}$	$5.24^{+2.97}_{-2.91}$	1.8	-1.26	1.54

Table 4: Constraints on the parameters \hat{H}_0 and A in the Fourier parameterization (5.8). Remember that Base+PantheonPlus and Base+Union3 reach up to $z = 2.3$ while Base+DES only up to $z = 1.13$. We compared the model to a constant H_0 and determine the Bayes factor B , ΔAIC and σ deviation. We see that the deviation from a constant is larger in σ 's than for the quadratic model. The ΔAIC is slightly better for the Fourier model than for a constant, although from the scale in [62] there is no preference to either model. The Bayes factors values account for a barely worth mentioning value according to the Jeffreys' scale [63], with the exception of the Base+DES data, which shows a substantial preference for the non constant model.

with only the two parameters \hat{H}_0 and A .

We now fit all the available bins showing the results in table 4. Figure ?? displays the fit for the 8 bins in the Base+PantheonPlus and Base+Union3 samples, and for only 6 bins in the Base+DES sample, remembering this data set has a reduced redshift range.

Again, table 4 includes the σ , ΔAIC and B values to see the robustness of this model against a constant H_0 . The parameter A is different from zero up to ~ 2.3 standard deviations, suggesting a preference for the non constant model. However, the scale in [62] states that the difference in AIC values is insufficient to favor any of the models. Table 4 also contains the results in each data set for only 6 bins, confirming a general improvement over the quadratic parameterization. On Jeffreys' scale [63], the Bayes factors in table 4 account for a barely worth mentioning value, with the exception of the Base+DES sample, where we found a substantial preference for the non constant model. It is interesting to note that the latest two bins in Base+PantheonPlus and Base+Union3 don't change too much the results in each data set compared to 6 bins.

5.3 Unbinned results

In Table 5 we show the fitted values of the cosmological parameters using the full redshift range of the data. For the Hubble constant we obtain an intermediate value between CMB and SH0ES of $H_0 \approx 70 \text{ km s}^{-1}\text{Mpc}^{-1}$, see figure 4. The constraints on w_0 and w_a are in good agreement with those found for DESI+SNe in [35]. Table 5 shows that a cosmological constant Λ (corresponding to $w_0 = -1$ and $w_a = 0$) as a source of DE is excluded at approximately 2σ with Base+Union3 and Base+DES data, while Base+PantheonPlus excludes it at approximately 1σ . Moreover, Ω_m agrees with the Planck value, $\Omega_m = 0.315 \pm 0.007$; however, the sound horizon r_d disagrees with the Planck value, $r_d = 147.09 \pm 0.26$, by about 1.5σ .

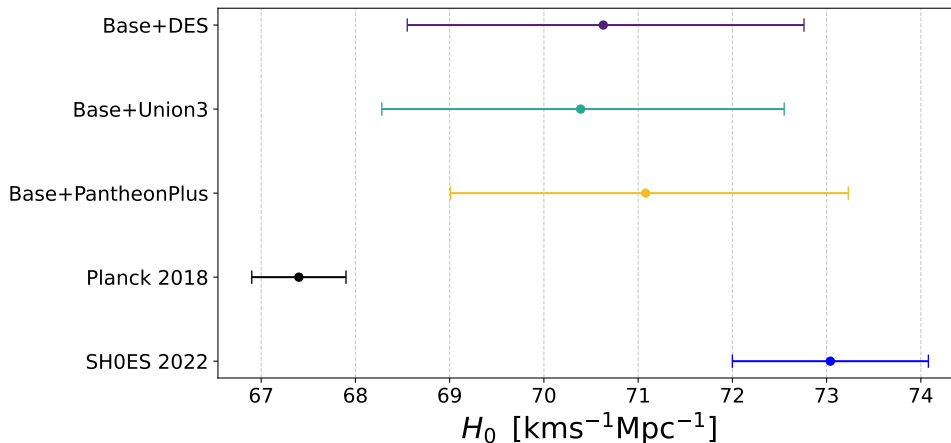


Figure 4: Estimates of the Hubble constant H_0 for the unbinned data set Base+PantheonPlus, Base+Union3 and Base+DES, compared to H_0 estimates for SH0ES [3] ($H_0 = 73.04 \pm 1.04 \text{ km s}^{-1}\text{Mpc}^{-1}$) and Planck 2018 team [1] ($H_0 = 67.4 \pm 0.5 \text{ km s}^{-1}\text{Mpc}^{-1}$).

Data	$H_0 \left[\frac{\text{km}}{\text{s Mpc}} \right]$	Ω_m	w_o	w_a	r_d [Mpc]
Base+PantheonPlus	$71.08^{+2.15}_{-2.07}$	0.31 ± 0.02	$-0.88^{+0.08}_{-0.07}$	$-0.45^{+0.58}_{-0.61}$	$140.95^{+4.29}_{-4.11}$
Base+Union3	$70.39^{+2.16}_{-2.11}$	0.33 ± 0.02	-0.68 ± 0.13	$-1.35^{+0.74}_{-0.78}$	$139.58^{+4.31}_{-4.13}$
Base+DES	$70.63^{+2.13}_{-2.08}$	0.33 ± 0.02	-0.75 ± 0.09	$-1.17^{+0.64}_{-0.66}$	$140.13^{+4.26}_{-4.20}$

Table 5: Best-fit values on the parameters H_0 , Ω_m , w_o , w_a and r_d of the megamasers+CC+DESI+SNe dataset, without binning and over the entire redshift range $z < 2.33$. Without the CC and megamasers data, H_0 , r_d and M cannot be determined. We see that the constraints on w_o and w_a resemble those in [35], for DESI + SNe data. A cosmological constant ($w_o = -1$ and $w_a = 0$) is excluded by $\sim 2\sigma$ when the SNe data are either Union3 or DES.

6 Summary and conclusions

In this work, we have studied the evolution in the value of H_0 with the redshift of the data used to determine it, finding a dynamic evolution in H_0 . For that we used the latest dataset of CC, megamaser, SNe Ia and BAO observations from the Year 1 data release of DESI. The results show that the Hubble tension, referring to a phenomenologically non-constant value in H_0 , cannot be resolved by the new DESI data together with a dynamical DE.

The SNe observations are chosen from one of the three most recent samples of Pantheon+, Union3 and DES. Pantheon+ and Union 3 share about 1360 SNe but differ in their analysis and treatment over systematics. DES has 1635 new SNe but share 194 low redshift SNe with Pantheon+. Our three data samples share the megamasers+CC+DESI data but differ in the SNe data. Base+PantheonPlus and Base+Union3 formed a total of 8 bins, and 6 bins for Base+DES.

If we consider only the first 6 bins, we found (see fig. 1), for the three samples, that H_0 decreases as a function of redshift for $z < 0.5$, and then rises in the region $0.5 < z < 0.9$ up to $\sim 78 \text{ km s}^{-1}\text{Mpc}^{-1}$. In fact, if we include bins 7 and 8, the dynamic trend becomes more robust, with H_0 decreasing again for these bins.

The results show a dynamical trend in H_0 with a statistical significance up to 1.5σ , for the quadratic parameterization (5.6) and up to 2.3σ for the Fourier parameterization (5.8), indicating a preference for a non constant model. However, the values in ΔAIC and the Bayes factor B , which penalize the extra parameters in the dynamical models, do not provide substantial support for the quadratic function against a constant value. From a Bayesian point of view, both the quadratic function and a constant H_0 fit the bins results equally well. Similar conclusions are obtained for the Fourier parameterization, except for the results of Base+DES, which have the highest ΔAIC and B values showing a substantial preference for the dynamical model, according to the Jeffrey’s scale.

Remarkably, the value of $\tilde{H}_0(z = 0)$ for both models, as shown in tables 3 and 4, is in complete agreement with that obtained by SH0ES, $H_0 = 73.04 \pm 1.04 \text{ km s}^{-1}\text{Mpc}^{-1}$.

We highlight that the three data sets, which use different SNe samples, show similar behaviors even though each sample differs in its content and methodology. Because of this, we can infer that this trend is not caused by uncountable systematic errors in the SNe parameters and it is more of an intrinsic behavior guided by the data.

We have ignored any calibration on either r_d or M . However, if we adopt them, we find that the bins values of H_0 are completely consistent with a constant. This would require to use data outside of the redshift bin, either CMB data to determine r_d or distance ladder data to determine M . As fixing r_d or M is equivalent to fixing H_0 from the beginning, which prevents the data from speaking for itself. It is relevant to highlight that any solution to the Hubble tension that only modifies the calibration of r_d or M won’t solve the tension presented here. In the unbinned case, in subsection 5.3 we obtained a r_d which is 1.5σ smaller than the one measured by Planck.

Of course, the results for H_0 may vary if one adopts a different binning strategy but we expect that the significance of the trend do not change significantly. This evolution in the Hubble constant might offer a new perspective on the Hubble tension. Since we’re using the $w_0w_a\text{CDM}$ model with very broad priors, it seems that a dynamical DE can’t remove this trend. Using a cosmological constant as the Dark Energy component only reduces the errorbars of the estimation of H_0 due to the reduced parameter space. This may increase the significance of the non constant models.

Some possible solutions would be either a hidden systematic error or some other assumption in the model. This could even be the reason why SH0ES and Planck have different values for H_0 given that they use data with different redshifts, but this needs further study, maybe considering H_0 not as an integration constant, but as a quantity dependent on the observed region of the Universe. Unfortunately, directly corroborating that the Hubble parameter at present time has different values depending on the region of the Universe is difficult, as due to the finiteness of the speed of light, we observe those regions in the past. However, nothing prevents us from thinking that just as there are perturbations to matter, these bring with them anisotropies in the expansion rate of the Universe with H_0 being more of an average value and the local departure of the cosmological principle [65–70].

Our binning strategy splits the data used, reducing the available data in each bin. This, combined with the decreasing quality in the data, produces large error bars in the inferred parameters which get worse at large z ’s. Therefore the quadratic and Fourier fittings present large uncertainties. We do not rule out that the constant H_0 be the correct result; we need to wait to improve the quality and number of the data to be able to reach a final conclusion.

The Hubble tension remains one of the most significant challenges in modern cosmology and astrophysics, highlighting persistent discrepancies in H_0 values derived from different

observational methods and across varied redshifts. This work contributes to the present discussion, providing further evidence that the Hubble tension is not only confined to early-versus late-time measurements but also appears consistently within purely late-time measurements reflecting unresolved aspect of cosmological models and data calibration.

Acknowledgments

The authors thankfully acknowledge Sebastien Fromenteau for his useful comments in the development of this work. M. L. H. was supported by Conahcyt grant 806098.

References

- [1] Planck Collaboration, Aghanim, N. et al., *Planck 2018 results - vi. cosmological parameters*, *A&A* **641** (2020) A6.
- [2] S. Alam, M. Aubert, S. Avila et al., *Completed sdss-iv extended baryon oscillation spectroscopic survey: Cosmological implications from two decades of spectroscopic surveys at the apache point observatory*, *Phys. Rev. D* **103** (2021) 083533.
- [3] A.G. Riess, W. Yuan, L.M. Macri et al., *A comprehensive measurement of the local value of the hubble constant with 1 km s⁻¹ mpc⁻¹ uncertainty from the hubble space telescope and the sh0es team*, *The Astrophysical Journal Letters* **934** (2022) L7.
- [4] J. Sakstein and M. Trodden, *Early dark energy from massive neutrinos as a natural resolution of the hubble tension*, *Phys. Rev. Lett.* **124** (2020) 161301.
- [5] A. Gogoi, R.K. Sharma, P. Chanda and S. Das, *Early mass-varying neutrino dark energy: Nugget formation and hubble anomaly*, *The Astrophysical Journal* **915** (2021) 132.
- [6] S.X. Tian and Z.-H. Zhu, *Early dark energy in k-essence*, *Phys. Rev. D* **103** (2021) 043518.
- [7] T.L. Smith, V. Poulin and M.A. Amin, *Oscillating scalar fields and the hubble tension: A resolution with novel signatures*, *Phys. Rev. D* **101** (2020) 063523.
- [8] R. Murgia, G.F. Abellán and V. Poulin, *Early dark energy resolution to the hubble tension in light of weak lensing surveys and lensing anomalies*, *Phys. Rev. D* **103** (2021) 063502.
- [9] A. Chudaykin, D. Gorbunov and N. Nedelko, *Combined analysis of planck and sptpol data favors the early dark energy models*, *Journal of Cosmology and Astroparticle Physics* **2020** (2020) 013.
- [10] Y. Wang, L. Pogosian, G.-B. Zhao and A. Zucca, *Evolution of dark energy reconstructed from the latest observations*, *The Astrophysical Journal Letters* **869** (2018) L8.
- [11] W. Yang, S. Pan, E. Di Valentino et al., *Observational constraints on one-parameter dynamical dark-energy parametrizations and the H₀ tension*, *Phys. Rev. D* **99** (2019) 043543.
- [12] R.-Y. Guo, J.-F. Zhang and X. Zhang, *Can the h₀ tension be resolved in extensions to λ cdm cosmology?*, *Journal of Cosmology and Astroparticle Physics* **2019** (2019) 054.
- [13] L. Amendola, *Coupled quintessence*, *Phys. Rev. D* **62** (2000) 043511.
- [14] S. Kumar, R.C. Nunes and S.K. Yadav, *Cosmological bounds on dark matter-photon coupling*, *Phys. Rev. D* **98** (2018) 043521.
- [15] W.L. Xu, C. Dvorkin and A. Chael, *Probing sub-gev dark matter-baryon scattering with cosmological observables*, *Phys. Rev. D* **97** (2018) 103530.
- [16] C.D. Kreisch, F.-Y. Cyr-Racine and O. Doré, *Neutrino puzzle: Anomalies, interactions, and cosmological tensions*, *Phys. Rev. D* **101** (2020) 123505.

- [17] R. D’Agostino and R.C. Nunes, *Measurements of H_0 in modified gravity theories: The role of lensed quasars in the late-time universe*, *Phys. Rev. D* **101** (2020) 103505.
- [18] Cruz, N. M. Jiménez and Escamilla-Rivera, Celia, *Late-time and big bang nucleosynthesis constraints for generic modified gravity surveys*, *Eur. Phys. J. Plus* **136** (2021) 51.
- [19] S. Mandal, D. Wang and P.K. Sahoo, *Cosmography in $f(q)$ gravity*, *Phys. Rev. D* **102** (2020) 124029.
- [20] E.D. Valentino, O. Mena, S. Pan et al., *In the realm of the hubble tension—a review of solutions**, *Classical and Quantum Gravity* **38** (2021) 153001.
- [21] J.L. Cervantes-Cota, S. Galindo-Uribarri and G.F. Smoot, *The unsettled number: Hubble’s tension*, *Universe* **9** (2023) .
- [22] L. Perivolaropoulos and F. Skara, *Challenges for λ cdm: An update*, *New Astronomy Reviews* **95** (2022) 101659.
- [23] K.C. Wong, S.H. Suyu, G.C.-F. Chen et al., *H0LiCOW – XIII. A 2.4 per cent measurement of H_0 from lensed quasars: 5.3 σ tension between early- and late-Universe probes*, *Monthly Notices of the Royal Astronomical Society* **498** (2019) 1420.
- [24] Millon, M., Galan, A., Courbin, F. et al., *Tdcosmo - i. an exploration of systematic uncertainties in the inference of h_0 from time-delay cosmography*, *A&A* **639** (2020) A101.
- [25] C. Krishnan, E.O. Colgáin, Ruchika, A.A. Sen, M.M. Sheikh-Jabbari and T. Yang, *Is there an early universe solution to hubble tension?*, *Phys. Rev. D* **102** (2020) 103525.
- [26] E. Ó Colgáin, M. Sheikh-Jabbari, R. Solomon et al., *Putting flat λ cdm in the (redshift) bin*, *Physics of the Dark Universe* **44** (2024) 101464.
- [27] M. Malekjani, R. Mc Conville, E. Ó Colgáin et al., *On redshift evolution and negative dark energy density in pantheon + supernovae*, *The European Physical Journal C* **84** (2024) 317.
- [28] M.G. Dainotti, B.D. Simone, T. Schiavone et al., *On the hubble constant tension in the sne ia pantheon sample*, *The Astrophysical Journal* **912** (2021) 150.
- [29] J.P. Hu and F.Y. Wang, *Revealing the late-time transition of H_0 : relieve the Hubble crisis*, *Monthly Notices of the Royal Astronomical Society* **517** (2022) 576.
- [30] Jia, X. D., Hu, J. P. and Wang, F. Y., *Evidence of a decreasing trend for the hubble constant*, *A&A* **674** (2023) A45.
- [31] X.D. Jia, J.P. Hu and F.Y. Wang, *Uncorrelated estimations of h_0 redshift evolution from desi baryon acoustic oscillation observations*, **2406.02019**.
- [32] M.G. Dainotti, B. De Simone, T. Schiavone et al., *On the evolution of the hubble constant with the sne ia pantheon sample and baryon acoustic oscillations: A feasibility study for grb-cosmology in 2030*, *Galaxies* **10** (2022) .
- [33] E. Ó Colgáin, M.M. Sheikh-Jabbari, R. Solomon, G. Bargiacchi, S. Capozziello, M.G. Dainotti et al., *Revealing intrinsic flat Λ CDM biases with standardizable candles*, *Phys. Rev. D* **106** (2022) L041301.
- [34] C. Krishnan, E. Ó Colgáin, M.M. Sheikh-Jabbari and T. Yang, *Running hubble tension and a h_0 diagnostic*, *Phys. Rev. D* **103** (2021) 103509.
- [35] DESI collaboration, *DESI 2024 VI: Cosmological Constraints from the Measurements of Baryon Acoustic Oscillations*, **2404.03002**.
- [36] M. Chevallier and D. Polarski, *Accelerating universes with scaling dark matter*, *International Journal of Modern Physics D* **10** (2001) 213.
- [37] E.V. Linder, *Exploring the expansion history of the universe*, *Phys. Rev. Lett.* **90** (2003) 091301.

- [38] R. Jimenez and A. Loeb, *Constraining cosmological parameters based on relative galaxy ages*, *The Astrophysical Journal* **573** (2002) 37.
- [39] D.W. Pesce, J.A. Braatz, M.J. Reid, J.J. Condon, F. Gao, C. Henkel et al., *The megamaser cosmology project. xi. a geometric distance to cgcg 074-064*, *The Astrophysical Journal* **890** (2020) 118.
- [40] D.W. Pesce, J.A. Braatz, M.J. Reid et al., *The megamaser cosmology project. xiii. combined hubble constant constraints*, *The Astrophysical Journal Letters* **891** (2020) L1.
- [41] W.D. Kenworthy, D. Scolnic and A. Riess, *The local perspective on the hubble tension: Local structure does not impact measurement of the hubble constant*, *The Astrophysical Journal* **875** (2019) 145.
- [42] M.J. Reid, D.W. Pesce and A.G. Riess, *An improved distance to ngc 4258 and its implications for the hubble constant*, *The Astrophysical Journal Letters* **886** (2019) L27.
- [43] C. Zhang, H. Zhang, S. Yuan, S. Liu, T.-J. Zhang and Y.-C. Sun, *Four new observational $h(z)$ data from luminous red galaxies in the sloan digital sky survey data release seven*, *Research in Astronomy and Astrophysics* **14** (2014) 1221.
- [44] R. Jimenez, L. Verde, T. Treu and D. Stern, *Constraints on the equation of state of dark energy and the hubble constant from stellar ages and the cosmic microwave background**, *The Astrophysical Journal* **593** (2003) 622.
- [45] J. Simon, L. Verde and R. Jimenez, *Constraints on the redshift dependence of the dark energy potential*, *Phys. Rev. D* **71** (2005) 123001.
- [46] M. Moresco, A. Cimatti, R. Jimenez et al., *Improved constraints on the expansion rate of the universe up to $z \sim 1.1$ from the spectroscopic evolution of cosmic chronometers*, *Journal of Cosmology and Astroparticle Physics* **2012** (2012) 006.
- [47] M. Moresco, L. Pozzetti and A.C. others, *A 6% measurement of the hubble parameter at $z \sim 0.45$: direct evidence of the epoch of cosmic re-acceleration*, *Journal of Cosmology and Astroparticle Physics* **2016** (2016) 014.
- [48] A.L. Ratsimbazafy, S.I. Loubser, S.M. Crawford et al., *Age-dating luminous red galaxies observed with the Southern African Large Telescope*, *Monthly Notices of the Royal Astronomical Society* **467** (2017) 3239.
- [49] D. Stern, R. Jimenez, L. Verde, M. Kamionkowski and S.A. Stanford, *Cosmic chronometers: constraining the equation of state of dark energy. i: $H(z)$ measurements*, *Journal of Cosmology and Astroparticle Physics* **2010** (2010) 008.
- [50] N. Borghi, M. Moresco and A. Cimatti, *Toward a better understanding of cosmic chronometers: A new measurement of $h(z)$ at $z \sim 0.7$* , *The Astrophysical Journal Letters* **928** (2022) L4.
- [51] M. Moresco, *Raising the bar: new constraints on the Hubble parameter with cosmic chronometers at $z \sim 2$* , *Monthly Notices of the Royal Astronomical Society: Letters* **450** (2015) L16.
- [52] M. Moresco, R. Jimenez, L. Verde, A. Cimatti and L. Pozzetti, *Setting the stage for cosmic chronometers. ii. impact of stellar population synthesis models systematics and full covariance matrix*, *The Astrophysical Journal* **898** (2020) 82.
- [53] D. Brout et al., *The pantheon+ analysis: Cosmological constraints*, *The Astrophysical Journal* **938** (2022) 110.
- [54] DES Collaboration, T.M.C. Abbott et al., *The dark energy survey: Cosmology results with 1500 new high-redshift type ia supernovae using the full 5-year dataset*, **2401.02929**.
- [55] D. Rubin, G. Aldering, M. Betoule et al., *Union through unity: Cosmology with 2,000 sne using a unified bayesian framework*, **2311.12098**.

- [56] D.M. Scolnic, D.O. Jones, A. Rest et al., *The complete light-curve sample of spectroscopically confirmed sne ia from pan-starrs1 and cosmological constraints from the combined pantheon sample*, *The Astrophysical Journal* **859** (2018) 101.
- [57] D. Foreman-Mackey, D.W. Hogg, D. Lang and J. Goodman, *emcee: The mcmc hammer*, *Publications of the Astronomical Society of the Pacific* **125** (2013) 306.
- [58] R. Trotta, *Bayes in the sky: Bayesian inference and model selection in cosmology*, *Contemp. Phys.* **49** (2008) 71 [0803.4089].
- [59] J. Skilling, *Nested sampling for general bayesian computation*, *Bayesian Analysis* **1** (2006) 833.
- [60] W.J. Handley, M.P. Hobson and A.N. Lasenby, *PolyChord: nested sampling for cosmology*, *Mon. Not. Roy. Astron. Soc.* **450** (2015) L61 [1502.01856].
- [61] H. Akaike, *A new look at the statistical model identification*, *IEEE Transactions on Automatic Control* **19** (1974) 716.
- [62] K.P. Burnham and D.R. Anderson, *Multimodel inference: Understanding aic and bic in model selection*, *Sociological Methods & Research* **33** (2004) 261.
- [63] H. Jeffreys, *The theory of probability*, OUP Oxford (1998).
- [64] D. Tamayo and J.A. Vazquez, *Fourier-series expansion of the dark-energy equation of state*, *Mon. Not. Roy. Astron. Soc.* **487** (2019) 729 [1901.08679].
- [65] J.P. Hu, X.D. Jia, J. Hu and F.Y. Wang, *Hints of new physics for the hubble tension: violation of cosmological principle*, **2410.06450**.
- [66] A. Heinesen and H.J. Macpherson, *A prediction for anisotropies in the nearby hubble flow*, *Journal of Cosmology and Astroparticle Physics* **2022** (2022) 057.
- [67] K. Bolejko, M.A. Nazer and D.L. Wiltshire, *Differential cosmic expansion and the hubble flow anisotropy*, *Journal of Cosmology and Astroparticle Physics* **2016** (2016) 035.
- [68] Hu, J. P., Wang, Y. Y., Hu, J. and Wang, F. Y., *Testing the cosmological principle with the pantheon+ sample and the region-fitting method*, *A&A* **681** (2024) A88.
- [69] Böhringer, Hans, Chon, Gayoung and Collins, Chris A., *Observational evidence for a local underdensity in the universe and its effect on the measurement of the hubble constant*, *A&A* **633** (2020) A19.
- [70] Schwarz, D. J. and Weinhorst, B., *(an)isotropy of the hubble diagram: comparing hemispheres*, *A&A* **474** (2007) 717.